Supporting Information
Surface-Engineered Nanomaterials as X-ray Absorbing Adjuvant Agents for Auger-Mediated Chemo-Radiation

Sang-Min Lee,[†‡] De-Hao Tsai,[†] Vincent A. Hackley,[†] Martin W. Brechbiel,[‡] and Robert F. Cook[†]*

[†]Material Measurement Laboratory, National Institute of Standards and Technology, Gaithersburg, Maryland 20899. [‡]National Cancer Institute, National Institutes of Health, Bethesda, Maryland 20892, United States.

CORRESPONDING AUTHOR EMAIL: robert.cook@nist.gov

1. Experimental Section

1.1 Materials. (±)-*α*-Lipoic acid, *cis*-diammineplatinum(II) dichloride (cisplatin), *N*,*N*-dicyclohexyl-carbodiimide (DCC), 4-(dimethylamino)pyridine (DMAP), trifluoroacetic acid (TFA), and all other reagents were purchased from Aldrich Chemical Co. (St. Louis, MO).[1] Amine-terminated poly(*t*-butyl acrylate) was purchased from Polymer Source Inc. (Quebec, Canada). Nominal 12-nm tannic acid-stabilized AuNPs were obtained from Ted Pella Inc. (Redding, CA) and used as received. Based on the extinction coefficient (ε) of AuNPs (133550×10^3 $M^{-1}cm^{-1}$ at λ_{max} = 517 nm) in water (information from http://www.tedpella.com/gold_html/NanoXact-gold.htm), the concentration of AuNPs was determined to be ≈ 6.144 nmol/L. Ultrapure deionized (DI, 18.2 MΩ-cm) water was obtained from a Model 2035BL Biological Grade Type I DI water purification system equipped with a reverse osmosis pretreatment system (Aqua Solutions, Inc., Jasper, GA).

1.2 Instrumental Analysis. Fourier-transform nuclear magnetic resonance (NMR) spectroscopy was performed on a GSX270 FT-NMR 270 MHz spectrometer (JEOL USA Inc., Peabody, MA). Chemical shifts of ^{1}H NMR spectra are reported in parts per million (ppm) against residual solvent resonance as the internal standard ($CDCl_3$ = 7.27 ppm, D_2O = 4.8 ppm).

UV-vis absorption spectra were obtained using a Lambda 750 spectrophotometer (Perkin Elmer, Waltham, MA).

Dynamic light scattering (DLS) and zeta-potential measurements were performed on a Zetasizer Nano ZS (Malvern Instruments, Malvern, U.K.) with a He-Ne laser (633 nm). Unless noted otherwise, all samples were dispersed in DI water for measurement. The data reported represent an average of 10 measurements with seven scans each; uncertainty is expressed as the standard deviation.

For agarose gel electrophoresis, 3 % (mass/volume) agarose gel (Agarose, Sigma) was prepared in 0.5× TBE buffer (Tris-Borate-EDTA buffer, Sigma). The gels were run in a horizontal electrophoresis system (EasyCast Mini Gel System, Thermo Scientific, Rochester, NY) at 150 V for 60 min.

Attenuated total reflectance-Fourier transform infrared (ATR-FTIR) spectroscopy was performed using a Nicolet Spectra 750 FTIR spectrometer equipped with a Thunder Dome Germanium ATR accessory (Thermo Scientific, Madison, WI). The ATR-FTIR spectra of each sample (Figure 3A in main text) were measured at pH ~6.0 to reduce the unexpected side reaction as well as to keep the

consistency of chemical environment. For sample preparation, AuNP sample solution was first concentrated to (8-20) μL (*i.e.*, at least 10× concentrated) by centrifugal filter (Amicon® Ultra-4 100k MWCO, Millipore, Billerica, MA) and then drop-cast onto the surface of a clean germanium ATR crystal. After evaporating the solvent in a clean bench at room temperature, a dry AuNP film was formed on the crystal surface. Spectra were collected from 128 scans with a resolution of 1 cm^{-1}.

Transmission electron microscopy (TEM) was performed on a Jeol JEM 1400 microscope operating at an accelerating voltage of 80 kV with LaB6 gun for the analyses of Pt^{II}-tethered gold nanoparticles.

X-ray photoelectron spectroscopy (XPS) measurements were performed with an AXIS $Ultra^{DLD}$ system (Kratos Analytical, Manchester, UK) using monochromatic Al Kα radiation with a pass energy of 150 eV. Samples were concentrated by centrifugal filtration (100k MWCO), drop-cast onto a Si wafer and dried overnight in the dark. Auger emissions from AuNPs and Pt^{II} pharmacophores were monitored by non-monochromatic Bremsstrahlung radiation. To identify the Auger lines of each element, their Auger parameters were compared to reference values because they are independent of the X-ray energy source used (Table S1).

Table S1. Auger parameters derived from the data in Figure 4.

Elements	Auger parameter (eV)[a]	
	Reported Value[b]	Measured Value[c]
Au ($4f_{7/2}$, $M_5N_{67}N_{67}$)	2099.7	2099.4
Pt ($4f_{7/2}$, $M_4N_{67}N_{67}$)	2108.6	2111.7

[a]Auger parameters are used to identify the Auger lines because they are independent of X-ray source used.
[b]Reference values from NIST XPS Database.
[c]Auger parameters derived by the equation: AP = BE($4f_{7/2}$) + KE($M_xN_{67}N_{67}$).

1.3. Preparation of Lipoic Acid-Terminated Poly(acrylic acid)

Lipoic acid-terminated poly(*t*-butyl acrylate) was first synthesized by reacting amine-terminated poly(*t*-butyl acrylate) (PAA, 125 μmol, M_m = 4 kDa, Polymer Source Inc., Dorval, QC, Canada) with lipoic acid (150 μmol, Aldrich) in a methylene chloride solution (50 mL) containing dicyclohexylcarbodiimide (DCC, 150 μmol) and a catalytic amount of 4-(dimethylamino) pyridine (DMAP). A schematic of the synthesis route is depicted in Scheme S1. The reaction mixture was stirred overnight at room temperature during which dicyclohexylurea formed as a precipitate. After the urea byproduct was removed by filtration, a 5-fold molar excess of trifluoroacetic acid (TFA) was added for the acid-catalyzed deprotection of *t*-butyl group (acidolysis) followed by stirring at room temperature for 3 days. After removal of dichloromethane and TFA by rotary evaporator, the lipoic acid-terminated poly(acrylic acid) was dissolved in DI water (10 mL) by adjusting the pH to 7.0 with aqueous NaOH (1 mol/L) and purified by dialysis (MWCO = 2 kDa, 10-mL cellulose ester membrane tube, Spectrum Laboratories, Inc.) against DI water for one week with a water change every 12 h. Water was then removed from the product solution by lyophilization to yield the yellowish product (255 mg, $M_m \cong 2.4$ kDa). The attachment of lipoic acid and removal of *tert*-butyl group were confirmed by ^1H NMR after acidolysis (Figure S1).

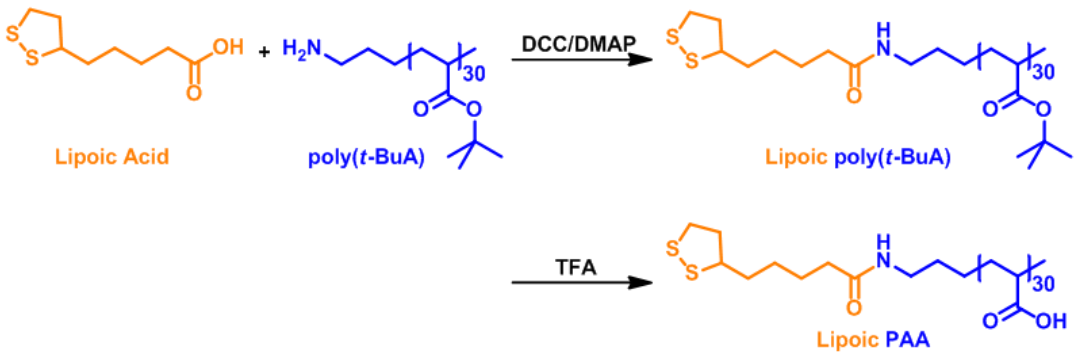

Scheme S1. Preparation of lipoic acid-terminated poly(acrylic acid) (Lipoic PAA).

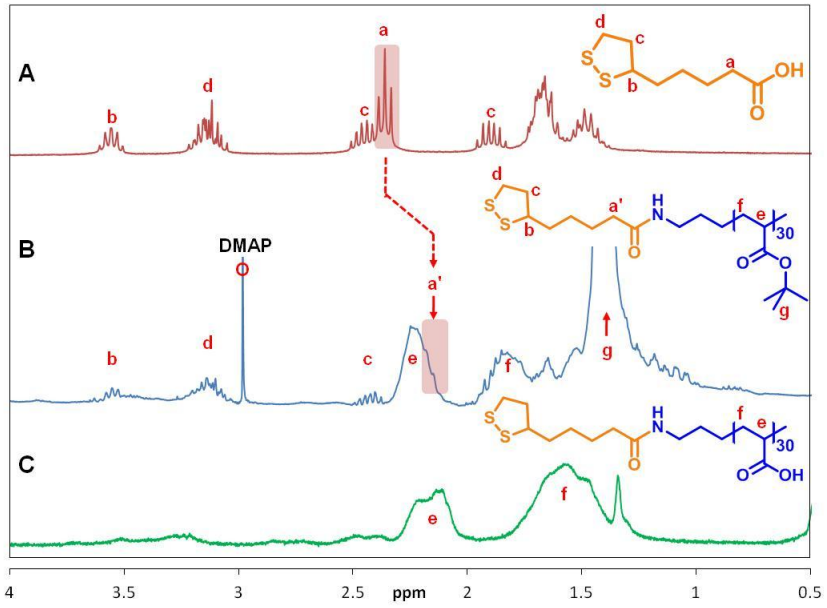

Figure S1. ^{1}H NMR spectra of (A) lipoic acid, (B) lipoic acid-terminated poly(*t*-butyl acrylic acid), and (C) lipoic acid-terminated poly(acrylic acid) after acidolysis.

1.4 Preparation of Poly(acrylic acid)-Conjugated Gold Nanoparticles (PAA-AuNPs). Gold nanoparticle (AuNP) solution (15 mL, 92.16 pmol) was added to lipoic-PAA solution (80 μL, 53.15 mmol/L, ≈ 6× relative to the number of surface gold atoms) and stirred overnight in the dark at room temperature.[1] After decreasing the volume of solution by centrifugal filtration (100 kDa MWCO), possible free unbound polymers were removed by dialysis (100 kDa MWCO, 5-mL cellulose ester membrane tube) against DI water.

1.5 Preparation of Platinum (II) Pharmacophore-Conjugated Gold Nanoparticles (Pt^{II}-AuNPs). To PAA-AuNP solution (5 mL, 78.4 pmol) was added *cis*-[$Pt^{II}(NH_3)_2(H_2O)_2$] (Pt^{II}, 1000, 2000, and 3000× relative to the number of AuNPs) followed by stirring in the dark at room temperature for 3 days. Then, unbound free Pt^{II} molecules were removed by centrifugal filtration (100 kDa MWCO) and washed with DI water.

1.6 Cell Culture.

a. Medium. Eagle's Minimum Essential Medium (EMEM) was purchased from ATCC (Manassas, VA). Trypsin solution (0.25 %, containing EDTA) was purchased from Invitrogen (San Diego, CA). Ca^{2+}- and Mg^{2+}-free phosphate-buffered saline (PBS, 1×) solutions were purchased from Mediatech (Manassas, VA).

b. Cell Lines. SK-OV-3 human ovarian cancer cells and MCF-7 human breast cancer cells were continuously cultured in EMEM supplemented with 10 % (v/v) heat-inactivated fetal bovine serum (FBS), at 37 °C in a humidified atmosphere containing 5 % CO_2.

1.7 Cytotoxicity Assays. The cells were seeded in 96-well plates (100 μL/well) with a concentration of 40,000 cells/mL in FBS-supplemented EMEM and were incubated to grow for 48 h. The media in the wells were replaced with the pre-made growth media containing the appropriate drug formulation (100 μL of solution at the appropriate Pt^{II} concentrations). The drug-treated cells were then incubated for 48 h and 72 h in a humidified atmosphere containing 5 % CO_2 at 37 °C, after which the cells were washed with PBS (2×, 250 μL). The cell viabilities were evaluated with CellTiter-Glo Luminescent Cell Viability Assay kit (Promega, Madison, WI). The relative cell survival percentages compared to the drug-free control (cells without any nanoparticles) were plotted against the total drug concentration on a logarithmic scale. The data reported represent an average of five measurements from different batches. The dose-response curves were obtained by sigmoidal logistic fitting using Origin 6.173 and the half-maximal inhibitory concentration (IC_{50}) values were determined on the basis of the fitted data.

2. Particle size, zeta potential, and stability tests of AuNPs

Table S2 summarizes the z-average hydrodynamic diameter (D_H) and zeta potential results. D_H of the PAA-AuNPs increased to (25.1 ± 3.9) nm (Figure S2 and Table S2) and a highly negative zeta potential (-64.7 ± 5.4) mV was observed. For comparison, lipoic acid-conjugated gold particles (lipoic-AuNPs) were also prepared and the D_H of lipoic-AuNPs was essentially unchanged (10.5 nm ± 1.9 nm) from that of the native AuNPs.

The calculated particle size distributions, determined from DLS using a non-negative constrained least squares inversion algorithm provided by the instrument vendor, are shown in Figure S2. The particle size increased significantly while the number of Pt^{II} atoms per AuNP on average (defined as Ω) is more than 2500, indicating AuNPs flocculated in solution. UV-vis results (Figure S3) confirm the observation by DLS.

Table S2. Size and Zeta Potential Results for AuNPs.

Samples (Pt^{II}/AuNP)	Hydrodynamic Diameter (nm)	Zeta Potential (mV)
Native AuNPs	10.4 ± 1.9	-24.4 ± 4.3
Lipoic AuNPs	10.5 ± 1.9	-41.8 ± 3.9
PAA-AuNPs	25.1 ± 3.9	-64.7 ± 5.4
Pt^{II}-AuNPs (0.7k)	21.2 ± 4.4	-54.3 ± 4.3
Pt^{II}-AuNPs (1.3k)	18.9 ± 3.3	-50.5 ± 4.8
Pt^{II}-AuNPs (>2.5k)	96.0 ± 58.1	N.D.[a]

[a] Not determined due to the high polydispersity.

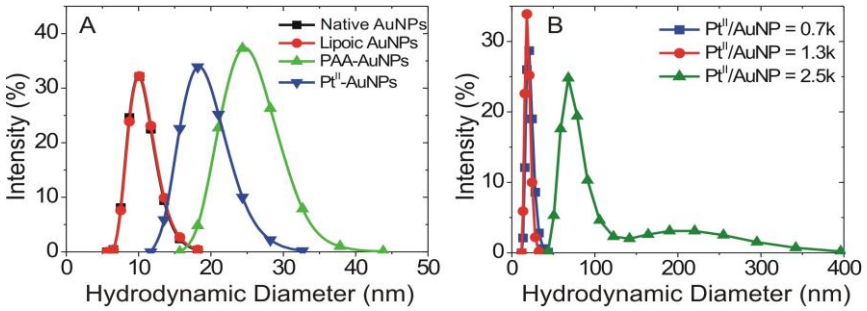

Figure S2. (A) Particle size distribution of AuNPs, with different types of coatings: lipoic acid-modified AuNPs (Lipoic AuNPs), PAA-modified AuNPs (PAA-AuNPs), and Pt^{II}-conjugated AuNPs (Pt^{II}-AuNPs) with Ω=1300. (B) Particle size distribution of Pt^{II}-AuNPs with various Ω values.

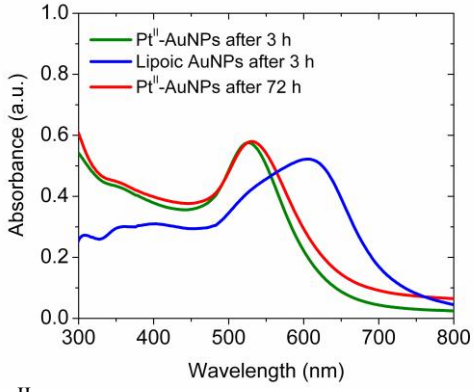

Figure S3. UV-Vis spectra of Pt^{II}-AuNPs and lipoic AuNPs in cell culture media at the corresponding incubation time.

3. ATR-FTIR Study

Figure S4 shows the ATR-FTIR spectrum for PAA-AuNPs at pH 8.0. Due to the deprotonation of PAA, the C=O stretching peak has disappeared completely while the peak intensity from COO^- anti-symmetric stretching (1552 cm^{-1}) is substantially increased with relatively low intensity for COO^- symmetric stretching (1409 cm^{-1}) as reported previously.[2]

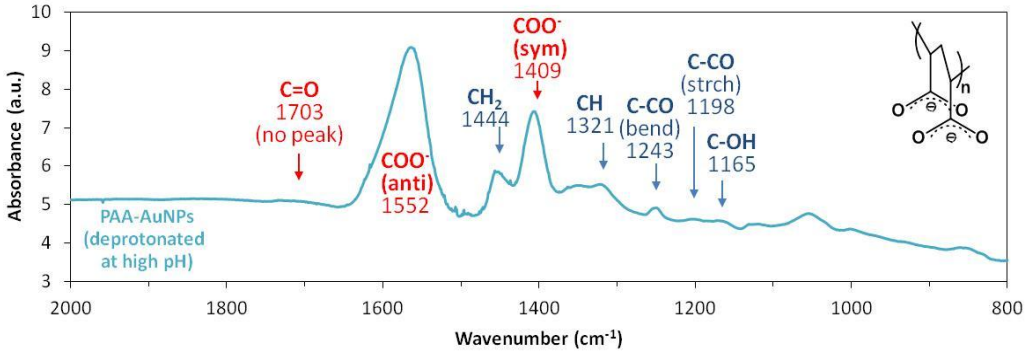

Figure S4. ATR-FTIR spectrum for PAA-AuNPs at pH 8.0.

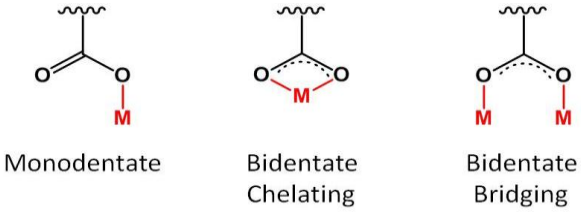

Scheme S2. Possible binding modes for metal carboxylate complexes.

4. XPS Study

Deconvoluted peaks in the C 1s region corresponds well with the chemical structure of lipoic-PAA. The Au 4f region contains a pair of peaks at 88.2 and 84.4 eV for $4f_{5/2}$ and $4f_{7/2}$, respectively, due to the spin-orbit coupling of Au 4f electrons. In the same manner, Pt 4f region shows a pair of peaks at 76.9 eV for $4f_{5/2}$ and 73.6 eV for $4f_{7/2}$. For comparison, Pt($4f_{7/2}$) peaks are observed at 73.2 eV for cisplatin (Pt^{II}), 70–71 eV for Pt^0, and 75–77 eV for Pt^{IV} compounds.

5. Determination of Pt^{II} concentration and release using colorimetric assay

The amount of Pt^{II} pharmacophore on AuNPs was determined using a modified literature procedure.[3] Briefly, an aliquot of Pt^{II}-AuNPs (100 μL) was added to aqueous HCl (2 N, 100 μL) and incubated for ≈ 3 h to release the Pt^{II} molecules from AuNPs and convert them to cisplatin while precipitating the agglomerated AuNPs. Then, the quantity of Pt^{II} was determined by colorimetric analysis using 10% $SnCl_2$-HCl (2 N) solution with UV-vis spectroscopy using the predetermined extinction coefficient (ε) of Sn-Pt complex (19062 $M^{-1}cm^{-1}$ at λ_{max} = 405 nm), which was obtained from the Pt^{II} standard solution and calibration curve (Figure S5).

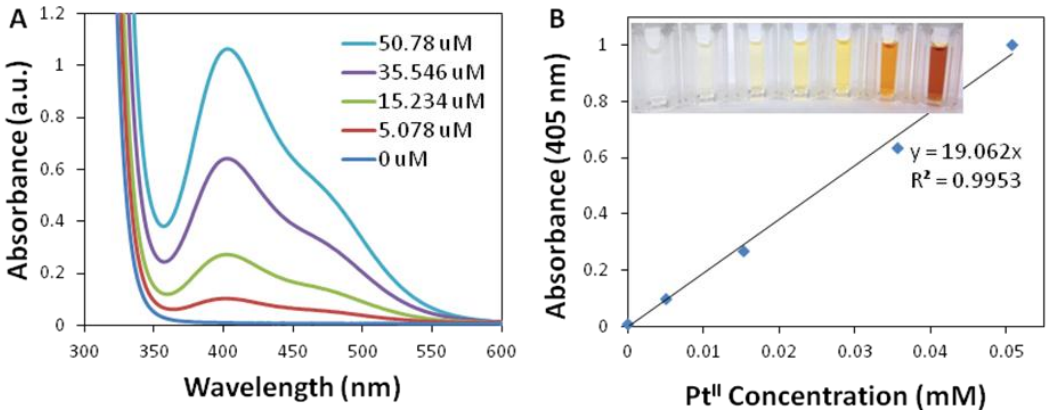

Figure S5. Colorimetric analysis of Pt^{II} concentration using 10 % $SnCl_2$-HCl solution. (A) UV-vis absorption spectra of $SnCl_2$-HCl solution with various concentrations of Pt^{II} standard solution. (B) The calibration curve for Pt^{II} ion obtained from the absorbance at λ = 405 nm.

6. Drug-release studies

Cumulative Pt^{II}-release amounts have been monitored under neutral (pH 7.4) and acidic (pH 5.0) condition at 37 ^{o}C (Figure S6). Because nanoparticles are internalized into the cells by endocytosis[4] and localized to perinuclear region through the acidified endosomes, the Pt^{II} pharmacophores can be released from the nanoparticles at the acidic environment of endosomes. Subsequently, the free small-molecule drugs, which possess moderate lipophilicity, can pass through endosomal membrane to interact with nuclear DNA. On the other hand, at physiological condition (pH 7.4), Pt^{II} should not be released for safe delivery to the target tissue.

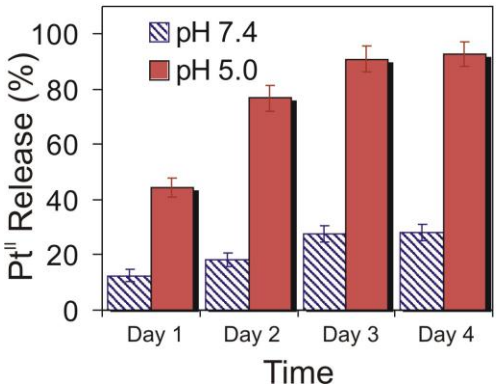

Figure S6. Cumulative release amount of Pt^{II} pharmacophore from Pt^{II}-AuNPs.

7. Cell viability studies with PAA-AuNPs

As shown in Figure S7, PAA-AuNP showed no apparent cytotoxicity up to a 3-day exposure. The results confirm that cytotoxicity is due to the addition of the Pt^{II} pharmacophore. The survival rate of cells without any nanoparticles is used as a control (i.e., 100 % cell viability at 0 μg/mL of AuNP, as shown in Figure. S7.

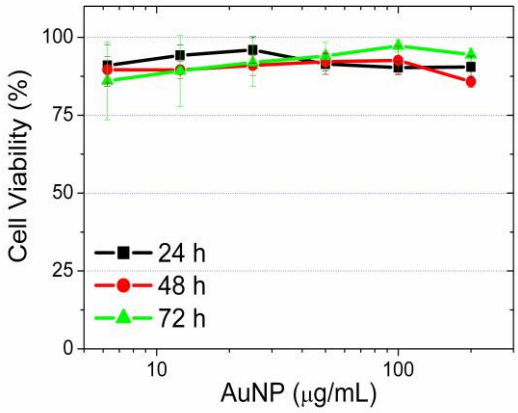

Figure S7. Cell viability studies with PAA-AuNPs

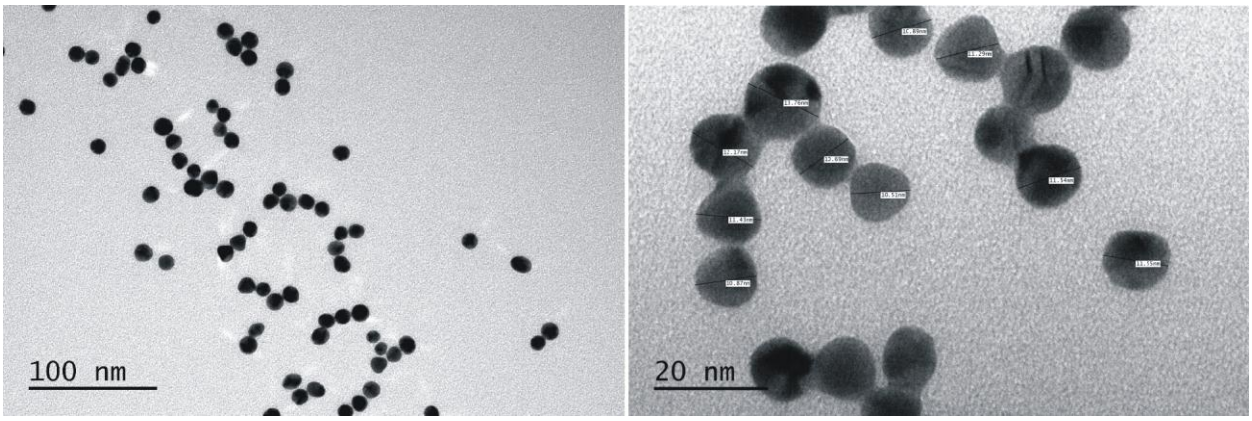

Figure S8. Transmission electron microscope images of Pt^{II}-AuNPs (Ω = 1.3k).

References

1. R. I. MacCuspie, A. M. Elsen, S. J. Diamanti, S. T. Patton, I. Altfeder, J. D. Jacobs, A. A. Voevodin and R. A. Vaia, *Appl. Organomet. Chem.* , 2010, **24**, 590-599.
2. J. Petroski and M. A. El-Sayed, *J. Phys. Chem. A*, 2003, **107**, 8371-8375.
3. O. I. Milner and G. F. Shipman, *Anal. Chem.*, 1955, **27**, 1476-1478.
4. R. A. Petros and J. M. DeSimone, *Nat. Rev. Drug Discov.*, 2010, **9**, 615-627.

Enlarged figures for more legibility:

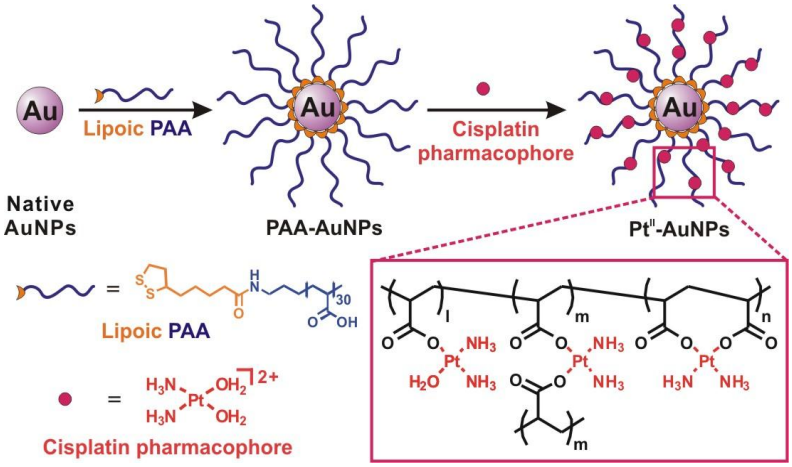

Scheme 1. Preparation of Cisplatin Pharmacophore–Tethered Gold Nanoparticles (Pt^{II}–AuNPs).

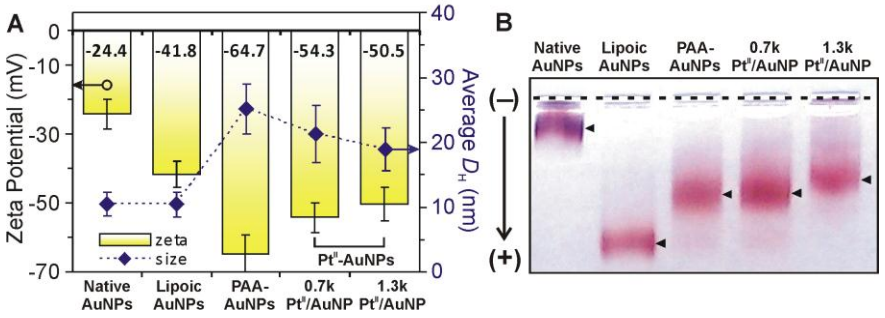

Figure 1. (A) Zeta potential and average hydrodynamic diameter (D_H) of native AuNPs, lipoic acid–modified AuNPs (lipoic AuNPs), PAA–AuNPs, and Pt^{II}–AuNPs with 0.7k and 1.3k Pt^{II}/AuNP ratio (Ω). (B) The corresponding electro-phoretic migration of modified AuNPs in 3 % agarose gel (150 V, 60 min).

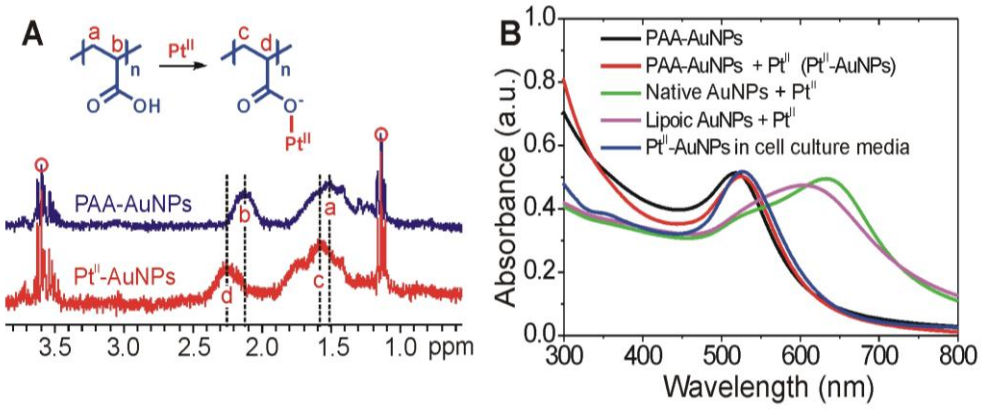

Figure 2. (A) ^{1}H NMR spectra of PAA–AuNPs and Pt^{II}–AuNPs. The circled peaks are due to the trace amount of ethanol, added to D_2O as a reference. (B) SPR spectra of AuNPs measured by UV–vis absorption.

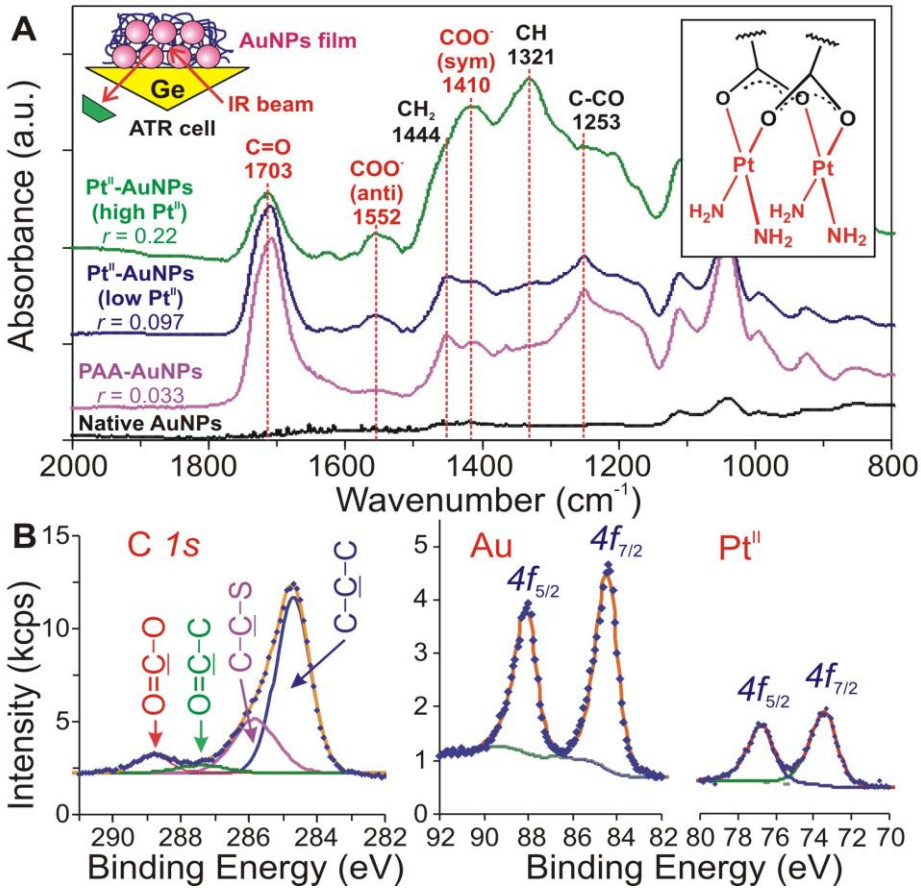

Figure 3. (A) Attenuated total reflectance-Fourier transform infrared (ATR-FTIR) spectra of tannic acid–stabilized (native) AuNPs, PAA–AuNPs, and Pt^{II}–AuNPs with Pt^{II}/AuNP ratio of 0.7k (low Pt^{II}) and 1.3k (high Pt^{II}). The intensity ratio (r) was determined by the ratio of the intensity of $(COO^{-})_{anti}$ to the intensity of (C=O). Left inset: Schematic picture of Ge crystal ATR cell, where AuNP samples were deposited by drop–casting. Right inset: Possible Pt^{II}–binding mode on PAA in Pt^{II}–AuNPs. (B) XPS spectra for C 1s, Au 4f, and Pt 4f regions collected from Pt^{II}–AuNPs.

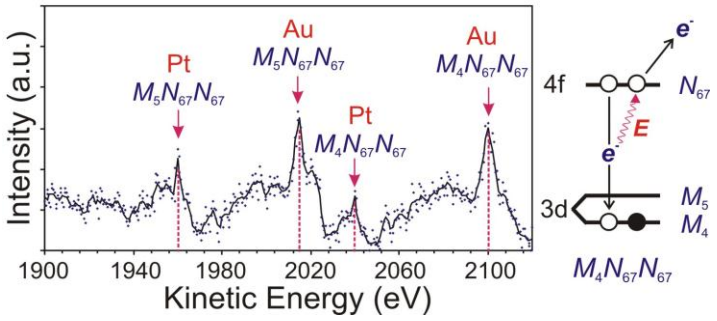

Figure 4. Electron kinetic energy spectrum of Auger emission from Pt^{II}–AuNPs. Each peak was identified by comparing to the NIST XPS Database.

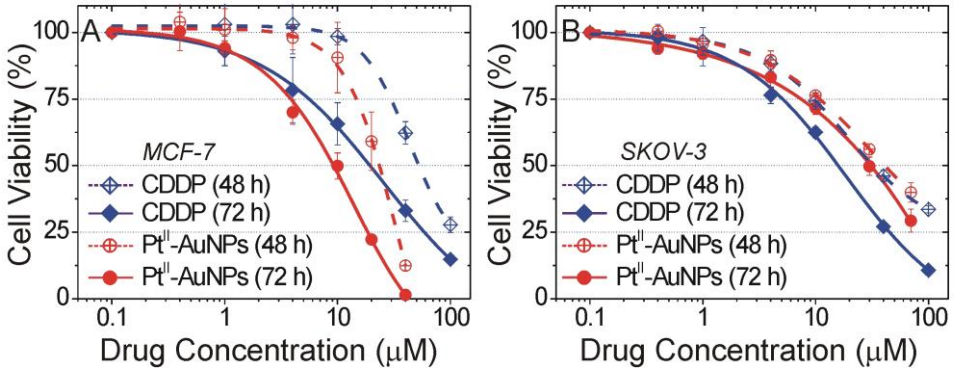

Figure 5. In vitro cytotoxicity profiles of Pt^{II}–AuNPs and cisplatin (CDDP) with MCF–7 breast cancer and SKOV–3 ovarian cancer cells.